# CORROSION BEHAVIOUR OF 2024 T351 AND 6056 T6 ALUMINIUM ALLOYS IN CHLORIDE SOLUTION

**Valérie GUILLAUMIN and Georges MANKOWSKI**

Laboratoire de Cristallochimie, Réactivité et Protection des Matériaux,
UPRESA CNRS 5071, ENSCT, 118 route de Narbonne, 31077 Toulouse Cedex 04, France

ABSTRACT The corrosion behaviour of 2024 T351 and 6056 T6 aluminium alloys was studied in chloride solutions. The polarization curve of 2024 alloy showed two breakdown potentials. The first was related to the dissolution of coarse intermetallic $Al_2CuMg$ particles, the second to the development of pitting and intergranular corrosion. For 6056 alloy only one breakdown potential was observed. It was related to pitting and intergranular corrosion. Intergranular corrosion developed on pit walls, and Al-Mg-Si-containing particles appeared to be pit nucleation sites.

**Keywords:** *Al 2024, Al 6056, pitting corrosion, intergranular corrosion, chloride.*

## 1. INTRODUCTION

The 2024 T3 alloy is used in the aircraft industry for numerous applications. Because of its attractive combination of mechanical properties and corrosion resistance, the 6056 alloy is currently being tested to evaluate whether it could replace the 2024 T3 alloy [1]. In this study, the corrosion behaviour of 2024 T351 and 6056 T6 alloys was investigated in 1M NaCl solution. The purpose was to compare the behaviour of the two alloys towards localized corrosion.

## 2. EXPERIMENTAL METHOD

Corrosion tests were performed on a 25 mm thick plate of 2024 T351 alloy and on a 3.2 mm thick sheet of 6056 T6 alloy. The composition of the alloys is given in Table 1. Before testing, the samples were polished with 1 µm diamond paste. All tests were performed at room temperature in aerated 1M NaCl (pH=6). Tests consisted of potentiokinetic polarization (sweep rate: 500 mV/h) of the samples from the cathodic potential of -900 mV/SCE to -400 mV/SCE. All potentials quoted are relative to a saturated calomel electrode. For several tests, scanning was stopped at different potentials, and the specimens were maintained at this final potential during various times.

After the tests, the samples were examined by optical microscopy and by scanning electron microscopy (SEM) using a JEOL JXA 6400 microscope. Observations by transmission electron microscopy (TEM) were also performed using a JEOL JM 2010 microscope, in order to examine precipitates and very small particles. Energy dispersed spectrometry (EDS) was also performed to analyse the precipitates.

Table 1. Composition of 2024 T351 and 6056 T6 alloys (wt%)

| | Al | Si | Fe | Cu | Mn | Mg | Cr | Zn | Ti | Zr |
|---|---|---|---|---|---|---|---|---|---|---|
| 2024 T351 | base | 0.06 | 0.17 | 4.54 | 0.63 | 1.51 | 0.01 | 0.08 | 0.03 | - |
| 6056 T6 | base | 0.92 | 0.19 | 0.87 | 0.55 | 0.86 | 0.004 | 0.15 | 0.02 | 0.1 |

## 3. EXPERIMENTAL RESULTS AND DISCUSSION

### 3.1 Microstructure of 2024 T351 and 6056 T6

Both optical and SEM observations allow two types of coarse intermetallic particles (with sizes that can reach 30 µm) to be distinguished in the 2024 alloy (Fig. 1): Al-Cu-Mg-containing particles and Al-Cu-Mn-Fe-containing particles. The first type was assigned to the $Al_2CuMg$

chemical combination (S phase) [2]. Observations by TEM revealed smaller particles. In the ma 1 µm long needle shaped $Al_2CuMg$ hardening precipitates (Fig. 2) and rod shaped $Al_{20}Mn$ dispersoids with an average size of a few micrometers were found. The dispersoid distribution very homogeneous in the whole matrix. However, the two types of coarse intermetallic part were surrounded by a dispersoid-free zone (Fig. 3). At the grain boundaries, hardening $Al_2C$ precipitates were found as were bigger needle shaped particles with an average length of 500 which can also be assigned to $Al_2CuMg$. No precipitate-free zone can be observed along the g boundaries (Fig.2). Both dispersoids and intergranular precipitates have already been observed analysed by other authors [2,3].

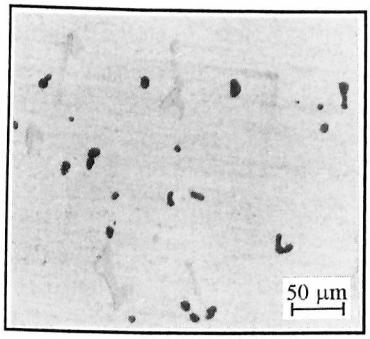


Fig. 1. Coarse intermetallic particles in 2024 T351 alloy.
Black : Al-Cu-Mg
Grey : Al-Cu-Mn-Fe.

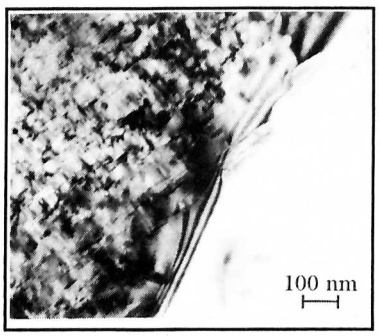


Fig. 2. Hardening $Al_2CuMg$ precipitates in the matrix close to a grain boundary.

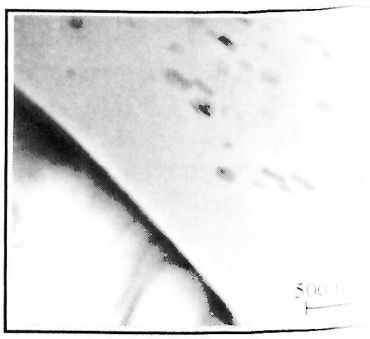

Fig. 3. Coarse intermetallic $Al_2CuMg$ particle surrounde by an $Al_{20}Mn_3Cu_2$ dispersoi free zone.

Two types of coarse intermetallic particles were also observed in the 6056 T6 alloy (Fig Al-Mg-Si-containing particles and Al-Si-Mn-Fe-containing particles reaching sizes of 15 Observations by TEM revealed the presence of Al-Mg-Si hardening precipitates (100 nm long Mn-Si-Mg-Cu-containing precipitates and Al-Zr-Si-Mg-Ti-Cu-containing precipitates (0.2 µm µm long) within the grain. Al-Mg-Si-Cu-containing precipitates were found in the grain bound (40 nm- 130 nm long). No precipitate-free zone can be observed along the grain boundaries (Fig Such precipitates have also been observed by C. Blanc et al. [4].

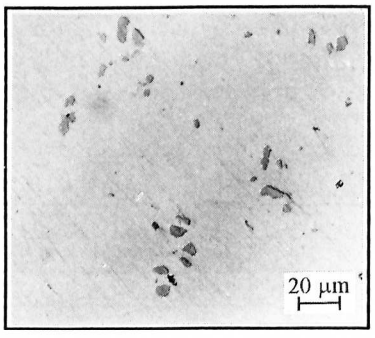


Fig. 4. Coarse intermetallic particles in 6056 T6 alloy.
Black : Al-Mg-Si
Grey : Al-Si-Mn-Fe.

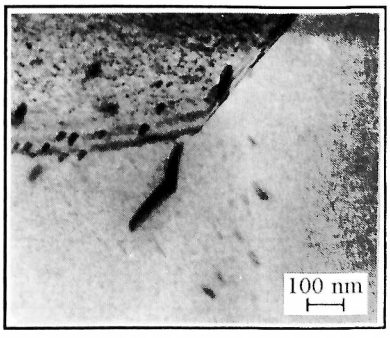


Fig. 5. Grain boundary in 6056 T6 alloy

### 3.2 Behaviour of 2024 T351 alloy in sodium chloride solution

Figure 6 shows the potentiokinetic polarization curve obtained in 1M NaCl solution for alloy 2024 T351. The curve shows two breakdown potentials: the more active one $E_{b1}$, close to -720 mV and the more noble one $E_{b2}$, close to -620 mV.

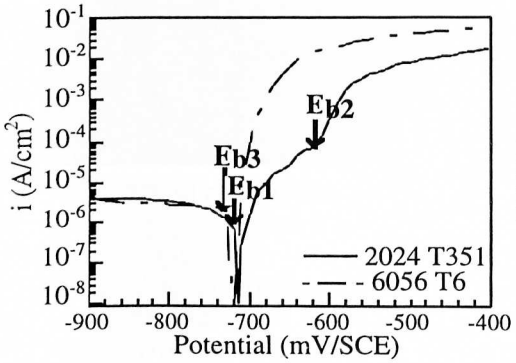


Fig. 6. Potentiokinetic polarization curve of 2024 T351 alloy and 6056 T6 alloy in 1M NaCl solution.

Figure 7 shows the remnant S phase particles after potentiokinetic polarization to -690 mV (i.e. 30 mV higher than $E_{b1}$). Some particles were severely attacked, and a resulting porous sponge-like structure covered by a more homogeneous layer can be observed. In the vicinity of the particles, the surrounding matrix was locally dissolved (Fig. 7b). On the contrary, the Al-Cu-Mn-Fe-containing particles, the matrix and the grain boundaries remained unattacked. The local dissolution of the matrix in the vicinity of the $Al_2CuMg$ particles also occurred during potentiokinetic polarization stopped before $E_{b1}$ whereas the S phase particles remained intact. So, the dissolution of the matrix surrounding the S phase particles is not a consequence of particle attack. So, the first breakdown potential is assumed to be caused by the dissolution of the $Al_2CuMg$ particles.

To understand matrix dissolution at the periphery of the S phase particles, observations by TEM were performed on intermetallic particles. Coarse $Al_2CuMg$ particles appeared to be surrounded by a $Al_{20}Mn_3Cu_2$ dispersoid-free zone. The dispersoid precipitation depletes the whole matrix of copper; likewise, the precipitation of the $Al_2CuMg$ coarse intermetallic particles leads to a preferential depletion of copper in the matrix surrounding the particles. As the dispersoids contain 15 wt % copper whereas the S phase particles contain 38 wt % copper, the depletion of the matrix surrounding the S phase particles is stronger than the depletion of the rest of the matrix. Indeed, the dispersoid-free zone has been found to contain 10-20 % less copper than the rest of the matrix. It can be assumed that the preferential dissolution of the matrix surrounding the coarse intermetallic particles is caused by the existence of a galvanic couple between the dispersoid-free zone and the rest of the matrix. Indeed, a galvanic couple between the precipitate and the matrix would cause the dissolution of the precipitate which is anodic in comparison to the matrix. Warner et al. [2] observed the same phenomenon on a 2024 T4 alloy. Moreover, Elboujdaini et al. [5,6] have shown that the presence of Mg-containing particles has a detrimental effect on the surrounding matrix dissolution and increases this phenomenon. According to these authors, the presence of Mg accelerates the cathodic reaction and leads to the formation of alkaline diffusion layers localized around the particles.

Finally, the local dissolution of the matrix surrounding the S phase particles is caused by a galvanic couple between the dispersoid-free zone and the rest of the matrix and can occur at low potential whereas the dissolution of the $Al_2CuMg$ precipitates occurs for potentials higher than $E_{b1}$ and can therefore lead, before the complete dissolution of the particle, to a sponge-like structure covered by a layer which appears to be more compact.

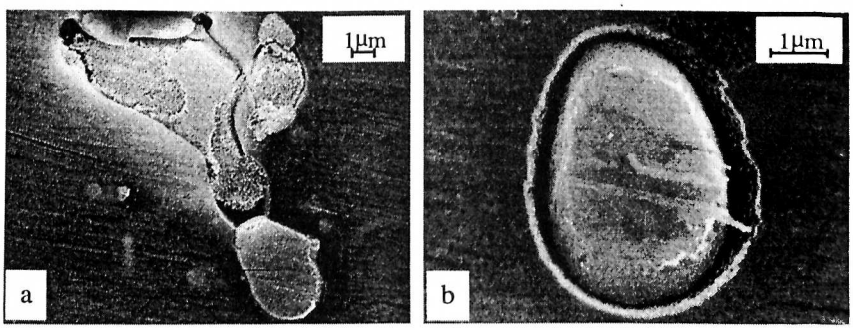


Fig. 7. S phase particles after potentiokinetic polarization to -690 mV, the potential was then maintained at -690 mV for 5 mn.

EDS analysis of the S phase particles after the potentiokinetic polarization to -690 showed a depletion of Mg (4.5 wt % instead of 15 wt % before the polarization), and an enrichm of copper (50 wt % instead of 38 wt %). This indicates that Mg selectively dissolves from $Al_2CuMg$ precipitates leaving Cu-rich remnants. This hypothesis was confirmed by potentiokin polarization to a potential of $E_{b1}$+30 mV in a NaCl solution acidified to pH 2. In these aggressive conditions, Mg dealloying was stronger. Indeed, there was no more Mg in the S ph particles, whereas the Cu content was about 60 wt %. These analyses were conducted on both porous sponge-like structure and the more homogeneous layer. There was no difference between two except the apparent structure of the layer which appeared to be less porous than the under particle. Actually, this layer may result from the superficial cold-work caused by mechan polishing.

After $E_{b2}$, both pitting and intergranular corrosion develop. Figure 8 presents several SE observations of a sample after potentiokinetic polarization to -610 mV (i.e. $E_{b2}$+10mV). Gr boundaries are attacked and large pits which show crystallographic facets develop within the gr (Fig. 8b).

According to the litterature [3,7], intergranular corrosion of Al-4%Cu alloys is caused by dissolution of the copper-depleted zone (0.2 wt % Cu) along the grain boundaries. However, fig 2 shows that no precipitate-free zone can be observed along the grain boundaries of the 2024 T3 alloy. Yet, EDS analysis shows that a zone of 20 nm wide on both sides of the grain bound contains 3 wt % Cu. Consequently, the grain boundary presents a slight depletion in copper comparison with the rest of the matrix which contains 4 wt % copper.

The dissolution of the $Al_2CuMg$ coarse intermetallic particles starts at -720 mV, so it can assumed that the dissolution of the $Al_2CuMg$ grain boundary precipitates, whose chemical type the same as that of the coarse intermetallic particles, occurs at a potential close to -720 m Anyway, -720 mV is 100 mV lower than –620 mV which corresponds to the second breakdo potential where intergranular corrosion can develop.

It can be assumed that $E_{b2}$ only corresponds to the matrix breakdown potential, since pits be observed on the sample surface, but it also allows intergranular corrosion to develop. After potential, grain boundaries are the preferential sites for the attack in so far as, on the one hand, previous dissolution of the intergranular precipitates makes the intergranular sites fragile, and the other hand, grain boundaries are more anodic in comparison to the rest of the matrix since only contain 3 wt % Cu.

Urushino et al. [3] who studied the intergranular stress corrosion cracking of 2024 alloy the behaviour of intermetallic compound $Al_2CuMg$ in 1M NaCl. They showed that its dissolut starts at -880 mV. In both cases (-880 mV or -720 mV), the two potentials are lower than $E_{b2}$, so intergranular precipitates must already be dissolved when the potential reaches -620 mV.

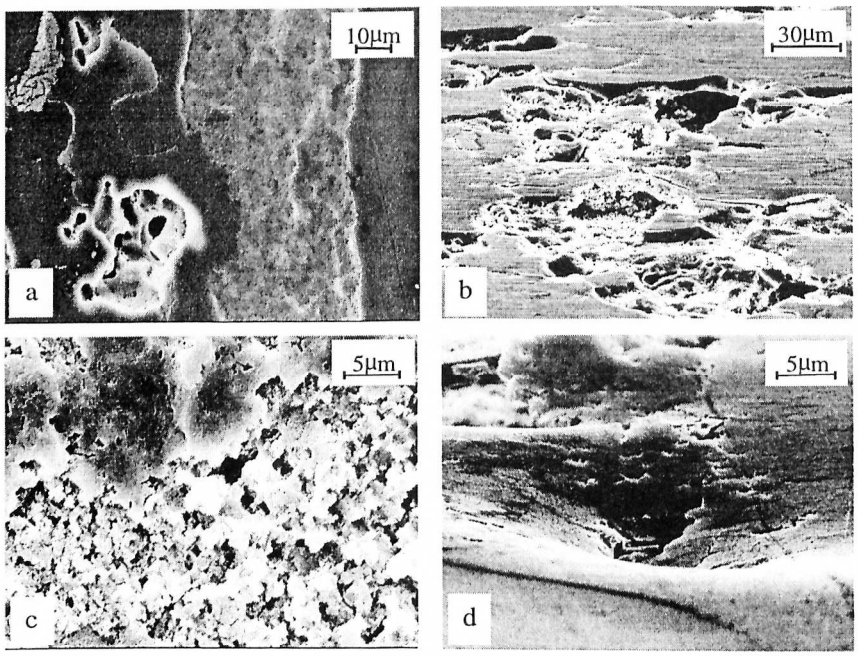


Fig. 8. 2024 T351 surface after potentiokinetic polarization to -610 mV, the potential was maintained at -610 mV for 5 mn. b and d were taken with an 88° tilt.

Finally, pitting and intergranular corrosion develop on and after the same breakdown potential which corresponds to the dissolution of the matrix both in the grains and in the grain boundaries where the precipitates have already been dissolved.

### 3.3 Behaviour of 6056 T6 alloy in sodium chloride solution

The polarization curve of 6056 T6 alloy in 1M NaCl solution shows only one breakdown potential $E_{b3}$ close to -730 mV (Fig. 6). After $Eb_3$ large pits can be observed as well as intergranular corrosion which takes place on pit walls (Fig. 9). When the attack becomes more severe, intergranular corrosion spreads from the pits but stays concentrated around them (Fig. 10). These two forms of corrosion seem to be dependent on each other. Zones where pits did not develop did not allow intergranular corrosion to develop, and remained completely unattacked.

Pits can reach a very large size (300 µm), they are significantly ramified presenting a rough profile (Fig. 10). They seem to grow following the model of Reigada *et al.* [8]. It is based on the idea that microscopic crystallographic tunnels are randomly nucleated on the pit wall, and quickly penetrate the metal. The occurrence and the size of the tunnels depend on local chloride concentration and the potential. Under mild conditions, tunnelling is a rare process, the size of the tunnels is small, so the pit profile becomes rough. With increasing aggressiveness, both the occurrence and the size of the tunnels increase leading to the formation of smooth, hemispherical pits.

The Al-Mg-Si coarse intermetallic particles were found to be strongly dissolved after a 5 mn immersion in 1M NaCl solution at free potential. Before a test, a large zone of a sample was examined by optical microscopy and all the precipitates were localized. After polarization to 10 mV higher than the corrosion potential, all the pits encountered in this zone nucleated on, or just around, the Al-Mg-Si-containing particles (Fig. 11). These particles can be considered as nucleation sites for pits and consequently for intergranular corrosion.

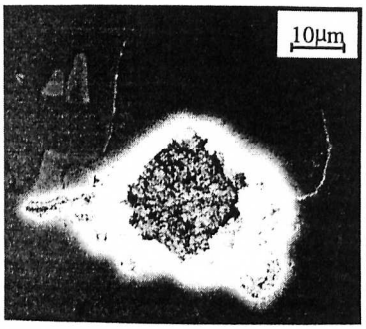


Fig. 9. Pit on 6056 T6 surface after potentiokinetic polarization to -700 mV, the potential was maintained for 5 mn at -700 mV.

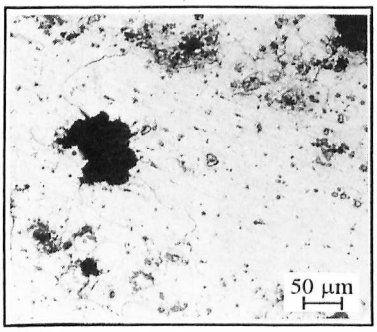


Fig. 10. 6056 T6 surface after potentiokinetic polarization to -400 mV.


Fig. 11. Al-Mg-Si-containing particle after potentiokinetic polarization of 6056 T6 alloy to -700mV, the potential was maintained for 5 mn at -700 mV

Some authors [1] have also observed that intergranular corrosion developed on pit walls of 6056 T6 alloy. Their observations revealed tall chimneys of corrosion products which led to the acidification of pit environment and allowed intergranular corrosion to develop.

## 4. CONCLUSION

The potentiokinetic polarization curve of alloy 2024 T351 presents two breakdown potentials. The more active one occurring around -720 mV is caused by the selective dissolution of the S phase particles. A severe dealloying of Mg results in the formation of Cu-rich particle remnants. The more noble one occurring around -620 mV corresponds to the development of both pitting and intergranular corrosion. This potential seems to correspond to the matrix breakdown potential. It also allows intergranular corrosion to develop. Grain boundaries are susceptible to preferential dissolution because they are more anodic in comparison to the rest of the matrix and the dissolution of the intergranular precipitates (around -720 mV) makes them fragile.

The potentiokinetic polarization curve of alloy 6056 T6 presents a breakdown potential which is related to the development of pitting and intergranular corrosion. The acidification of the environment leads to intergranular attack which takes place on the pit walls. The Al-Mg-Si containing precipitates were found to be pit nucleation sites.

Acknowledgements–This work was carried out in the framework of the " Laboratoire Régional pour l 'Amélioration des Matériaux Stucturaux pour l'Aéronautique " with the financial support of the Région Midi-Pyrénées. Special recognition goes to Michelle Reversat and Djar Oquab for the SEM work, and Josette Poujardieu for TEM work.

## REFERENCES

[1] T.D. Burleigh: 3rd International Conference on Aluminium Alloys (ed. L. Arnberg et al.) Trondheim, Norway (1993), 435.
[2] T.J. Warner, M.P. Schmidt, F. Sommer and D. Bellot : Z. Metallkd. 86(1995), 494.
[3] K. Urushino and K. Sugimoto: Corros. Sci. 19(1979), 225.
[4] C. Blanc and G. Mankowski: Corros. Sci. 39(1997), 949.
[5] M. Elboujdaini and E. Ghali: Corros. Sci. 30(1990), 855.
[6] M. Elboujdaini, E. Ghali, R.G. Barradas and M. Girgis : J. of Appl. Electrochem. 25(1995), 4
[7] J.R. Galvele and S.M. de Micheli : Corros. Sci. 10(1970), 795.
[8] R. Riegada, F. Sagues and J.M. Costa : J. Chem. Phys. 101(1994), 2329.